

On the role of solvent effects on the electronic transitions in Fe(II) and Ru(II) complexes

Sergi Saureu^a, Coen de Graaf^{a,b}

^a*Departament de Química Física i Inorgànica, Universitat Rovira i Virgili, Marcel·lí Domingo s/n, 43007 Tarragona, Spain*

^b*Institució Catalana de Recerca i Estudis Avançats (ICREA) Passeig Lluís Companys 23, 08010, Barcelona, Spain*

Abstract

Solvent effects on the vertical excitations of complexes with spin crossover are studied with CASPT2 and time-dependent DFT techniques. The geometry of the $[\text{Fe}(\text{phen})_3]^{2+}$ complex was optimized with DFT using the PBE0 functional, and subsequently, the absorption spectrum was calculated with CASPT2. The spectrum is in good agreement with experiment and the effects of the solvent were found to be small as long as the symmetry of the complex is maintained. The on-set of the MLCT band was found to be shifted by 0.4 eV, which we attribute to the lack of thermal motion in our treatment. The large solvent effects on some of the excitations in $\text{trans}(\text{Cl})\text{-Ru}(\text{bpy})\text{Cl}_2(\text{CO})_2$ are reproduced both with TD-DFT and CASPT2 through a COSMO or PCM treatment of the solvent.

Keywords: Absorption spectra ; ab initio calculations ; spin crossover ; solvent effects

1. Introduction

Over the last decades important advances have been made toward the synthesis of systems with bistability under normal conditions for which the switching is fast and both states sufficiently long-lived to take profit of the bistability. A system capable of persistently changing its magnetic or electric properties upon some external stimulation has many potential technological applications, for example to make nano-switches or as memory devices. In

Email address: coen.degraaf@urv.cat (Coen de Graaf)

this area of research, the compounds with an interconversion between two different spin states –spin crossover (SCO)– that can be triggered by a change in temperature, pressure or irradiation with light, form an important group. From the applicability point of view, the method that offers optimal control on the process is the light induced variant. This process, also known as light-induced excited spin state trapping (LIESST), was discovered in the 1980s [1, 2] and the basic mechanism was elucidated shortly afterwards [3, 4]. Important ingredients to explain the occurrence of LIESST are the energy difference between the high-spin (HS) and low-spin (LS) states; the vertical excitation energies of the metal-to-ligand charge transfer (MLCT) and ligand-field (LF) states; coordination degree of the ligand; cooperativity, among other factors [5–7].

Theoretical investigations have focussed on many of these aspects, but especially the determination of the energy difference between the HS and LS state has attracted much attention. The pioneering work of Paulsen and co-workers [8] established that standard density functional theory calculations are not accurate enough to precisely predict the stability of the HS state with respect to the LS state (ΔE_{HL}) in mononuclear SCO complexes. Over the past decade, significant evidence has accumulated that even the best current DFT functionals can display large errors for specific types of transition metal energetics. In particular, standard pure functionals (like LDA, BLYP, or PBE) systematically overstabilize low-spin states, while hybrid functionals (like B3LYP, or PBE0) overstabilize high-spin states due to the inclusion of a portion of Hartree-Fock exchange. The B3LYP* and OPBE functionals have emerged as most likely candidates for use in SCO complexes. Reiher and co-workers [9] suggested a reduction of the amount of HF exchange to 15% in B3LYP functional, B3LYP*, but this change is not successful for all iron compounds. Swart and co-workers studied different combinations of the exchange and correlation functionals and found that the OPBE functional [10, 11] which is the combination of Handy’s optimised exchange (OPTX) with the PBE correlation (PBEc) correctly predicts the lowest spin state in many transition-metal complexes. Therefore it is *a priori* unknown which amount of HF exchange is appropriate to give good results for transition-metal complexes.

There are also several studies devoted to SCO based on post Hartree-Fock methodologies. These strategies are based on a multiconfigurational description of the electronic structure and make possible to consider spin eigenfunctions, to treat ground and excited states on an equal footing, and

include spin-orbit coupling effects. A standard implementation of multiconfigurational self-consistent field (SCF) calculations is given by the complete active space (CASSCF) [12]. Combining CASSCF with multiconfigurational second-order perturbation theory (CASPT2) [13] results in a very successful computational scheme to treat transition metal complexes. The CASSCF wave function gives a good description of the electron distribution but lacks important dynamical electron correlation effects. This does not strongly affect the electron distribution but may give rise to rather large changes in the relative energies of the different electronic states. The complete active space second-order perturbation theory (CASPT2) accounts for dynamic electron correlation in the case of multiconfigurational wave functions of medium to large sized systems.

Since LIESST is intimately related to the local properties of the Fe(II) complex, especially to the first coordination sphere of the central metal, most theoretical studies take an isolated, *gas phase* molecule approach. The role of the environment (long-range electrostatic interactions, solvent effects) are less well-studied, although the study of Robert and co-workers for thermal SCO is a nice example how theory can quantify the effect of interactions that go beyond the simple isolated molecule description [14]. In the study of the SCO in Prussian-blue analogues it was found that the environment is actually the driving force for the HS-LS change [15]. One important ingredient of LIESST that is possibly strongly dependent on the description of the environment is the vertical excitation spectrum of the initial LS state. Actually, the study of the transient absorption spectroscopy study of Tribollet *et al.* on $[\text{Fe}(\text{phen})_3]^{2+}$ (phen=1,10-phenanthroline) points to important solvent effects on the excitation energies [16]. This was based on the mismatch of approximately 0.3 eV between the relative energies measured in experiment and those calculated for the related compound $[\text{Fe}(\text{bpy})_3]^{2+}$ (bpy=2,2'-bipyridine) with a multiconfigurational approach applied to the isolated complex [17, 18].

To settle the importance of the solvent effects on the vertical excitation spectrum and explain the difference in calculated and observed transition energies, we investigate the electronic states of $[\text{Fe}(\text{phen})_3]^{2+}$, trans(Cl)-Fe(bpy)Cl₂(CO)₂ and trans(Cl)-Ru(bpy)Cl₂(CO)₂ (depicted in Figure 1), comparing vacuum results with those obtained in a model that accounts for solvent effects. Furthermore, we compare time-dependent DFT to CASPT2 results in order to establish the viability of the simpler, and computationally more efficient DFT based method. The second and third complexes do not

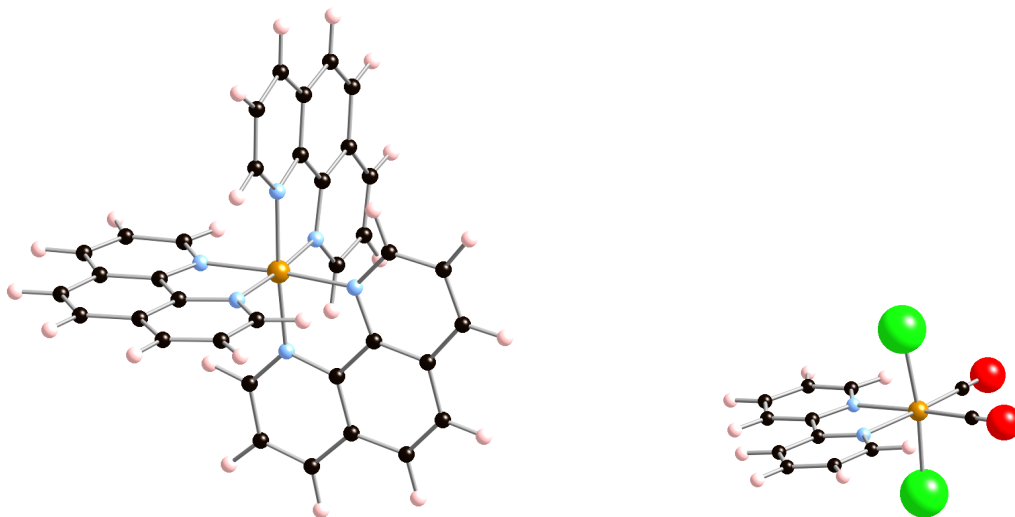


Figure 1: Ball and stick presentation of the complexes studied in this paper: (left) $[\text{Fe}(\text{phen})_3]^{2+}$ (**1**), (right) $\text{trans}(\text{Cl})\text{-Fe}(\text{bpy})\text{Cl}_2(\text{CO})_2$ (**2**) and $\text{trans}(\text{Cl})\text{-Ru}(\text{bpy})\text{Cl}_2(\text{CO})_2$ (**3**). Color code: orange for Fe and Ru, red for O, green for Cl, black for C, blue for N and pink for H.

belong to the class of SCO materials, but were chosen as benchmark models. The Ru-compound has recently been studied with TD-DFT and to some extent with CASPT2 [19] and shows important solvent effects, blue-shifting some specific MLCT states by approximately 1 eV.

2. Computational information

All geometries were optimized using the hybrid functional PBE0 [20], which adds 25% of exact Fock exchange to the standard PBE functional. This functional has been used previously, giving good results for the geometrical parameters for related SCO complexes [21, 22]. The molecular orbitals are expanded with the default triple- ζ basis set with one polarization function (def2-TZVP) [23].

The optimal geometry of the HS and LS states of the three complexes was determined by optimizing all geometrical variables without symmetry constraints and characterized as minima by a vibrational frequency calculation. The geometries used to build the energy potential curves of the ground state around the LS DFT geometry were generated from restricted geometry optimizations fixing the Fe-N distances at different values in an interval

of 1.8 to 2.0 Å. Time-dependent DFT calculations were performed with the PBE0 functional using the full random phase approximation (RPA) [24]. Additionally, calculations in solution were performed using H₂O or acetonitrile as solvent with the dielectric continuum model COSMO [25]. All DFT calculations were carried out using the TURBOMOLE package [26, 27] version 6.3.

CASSCF/CASPT2 calculations were performed as implemented in the MOLCAS 7.4 package [28, 29]. Atomic natural orbital (ANO) basis sets optimized for scalar relativistic effects and core correlation were applied for all atoms [30, 31]. For complex **1** we used a (7s,6p,5d,4f,3g,2h) contraction for Fe, (4s,3p,1d) for N, (3s,2p) for C and (2s) for H. For complex **2**, the ANO basis is the same but for C and O, which is (4s,3p,1d) and the basis set for Cl is contracted to (5s,4p,1d). Complex **3** has the same basis set contraction. The Cholesky decomposition [32, 33] was used to reduce the computational cost associated to the calculation of the two-electron integrals. Scalar relativistic effects were included using Douglas-Kross-Hess Hamiltonian [34]. Spin-orbit coupling and oscillator strengths of the electronic transitions were calculated with the state interaction approach [35, 36].

Different active spaces were used to construct the CASSCF reference wave function depending on the complex or the transitions studied. For complex **1** three active spaces were used that are graphically represented in Figure 2. The first active space contains 10 electrons distributed in all possible ways over 12 orbitals; five orbitals with mainly Fe-3d character, two σ -bonding orbitals with important contributions on the lone pairs of N, and five orbitals that account for the double shell effect of the 3d-shell, the so-called 3d' orbitals. This active space has been used in many applications on TM complexes before and provides a balanced description of all the important non-dynamic electron correlation [13, 36, 37]. The next active space extends the previous one with three ligand π^* orbitals leading to an active space of 15 orbitals and 10 electrons. The inclusion of these orbitals permits the study of MLCT states. Finally, the last active space was used to analyze the ligand-centered excitations in the π -system. It includes 12 ligand orbitals, six occupied ligand π orbitals and six unoccupied ligand π^* orbitals, for a total of 12 electrons. For complex **2** only one active space was used. It contains 10 electrons in 14 orbitals; the Fe-3d and 3d' orbitals, two σ -bonding ligand orbitals and two π^* orbitals of the carbonyl ligands. The inclusion of π^* orbitals of the pyridine ligand is unfortunately not possible without running into CAS spaces that are unmanageable in size. A similar problem occurs

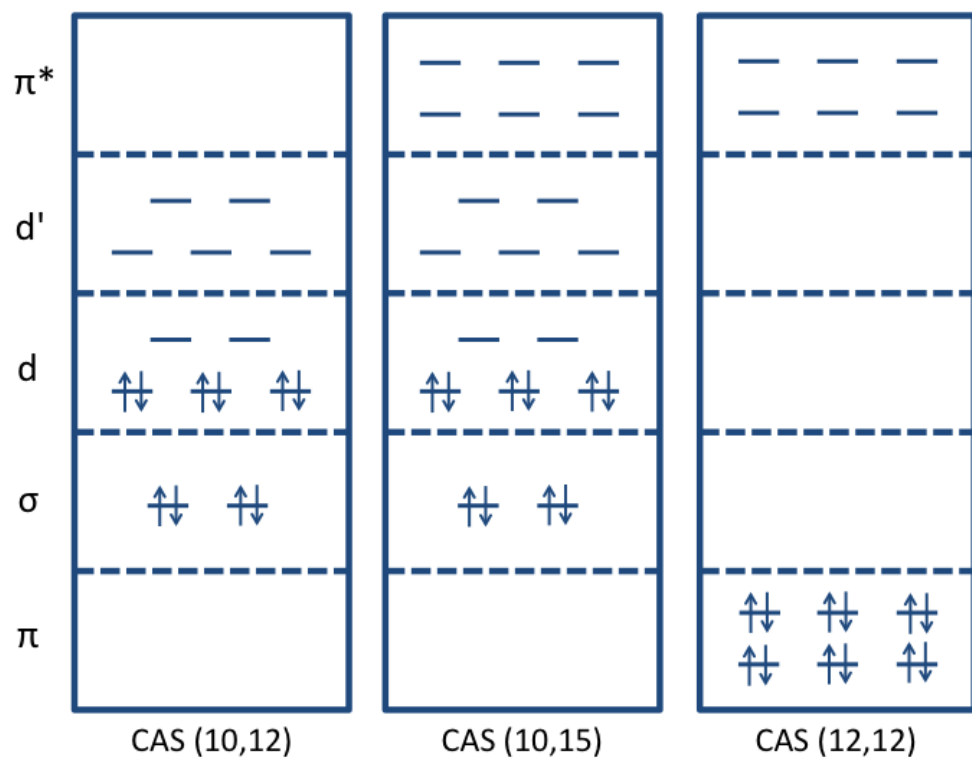


Figure 2: Schematic representation of the different active spaces used in the calculations for complex **1**.

for **3**. The study of Escudero and González on $\text{trans}(\text{Cl})\text{-Ru}(\text{bpy})\text{Cl}_2(\text{CO})_2$ showed that only with an active space of 22 electrons and 21 orbitals, excitations could be calculated involving the three different ligands. Here, we restrict ourselves to the excitations involving the pyridine ligand, which can be done with an active space of 14 electrons in 13 orbitals (5 Ru-4d orbitals, 4 pyridine π orbitals and 4 pyridine π^* orbitals). The active orbitals of all cases are graphically represented in the supporting information.

CASPT2 calculations account for the remaining electron correlation by correlating all the electrons except the deep core electrons ($1s^2$ for N and C and $1s^22s^22p^6$ for Fe). In order to exclude possible intruder states, we applied an imaginary level shift of 0.15-0.25 a.u. in CASPT2 [38]. The standard definition of the zeroth-order Hamiltonian was used throughout the calculations. It has been suggested in the literature that the IPEA shift in the zeroth-order Hamiltonian [39] should be increased when dealing with spin crossover compounds [40, 41] This is especially relevant when one is aiming at a precise determination of the adiabatic energy difference between the HS and LS state, which is a central quantity for thermal SCO. In the present study, we mainly focus on vertical excitation energies, for which the standard zeroth-order Hamiltonian performs very well, in general. The solvent effects were taken into account in the CASSCF/CASPT2 calculations with the polarizable continuum model (PCM)[42–44].

Finally, we have analyzed the wave function for all complexes in an orthogonal valence bond picture [45, 46]. For this purpose, the natural active orbitals are transformed into orthogonal localized orbitals with either exclusively Fe/Ru or ligand character following the procedure described in Ref. [47], which is based on pair-wise rotations of bonding and anti-bonding metal-ligand orbitals.

3. Results and Discussion

3.1. Geometries and adiabatic energy differences

The geometry of the isolated complex **1** was optimized for the three lowest electronic states with different spin coupling of the $3d^6$ manifold of the Fe^{2+} ion: singlet, triplet and quintet. The DFT calculations for the triplet and quintet were performed within the spin-unrestricted formalism, and hence, the resulting electronic states are not necessarily eigenfunctions of the \hat{S}^2 operator. However the spin functions considered here are essentially mono-determinantal and the spin contamination is very small. The expectation

values of \hat{S}^2 for HS and the intermediate spin state (triplet, IS), 6.02 and 2.03, are close to the formal values of 6 and 2.

In line with the findings of previous studies, the optimized bond lengths of **1** are slightly overestimated by 0.02 Å for LS and 0.05 Å for HS in comparison with the experimental values of 1.98 Å for LS and 2.15 Å [48]. This overestimation is caused by the hybrid functional used, the inclusion of 25% exact Fock exchange makes the bond slightly too weak [22]. Nevertheless, the bond elongation upon the LS to HS conversion of 0.2 Å is in agreement with experiment, as expected. The PBE0 HS and IS adiabatic energies with respect to the LS state are -0.15 eV and 0.51 eV for **1**, and 0.12 eV and 0.58 eV for **2**. The fact that both compounds have a LS ground state at low temperatures shows that the PBE0 functional tends to overstabilize the open-shell configurations with respect to the closed shell singlet state [10, 11, 49].

Additional optimizations were done taking into account the solvent effects, but neither water nor acetonitrile introduces significant changes in the geometries or relative energies. The Fe–N distances remain practically the same and the overstabilization of the HS state is reduced only by 0.06 eV, which does not repair the erroneous behaviour of the hybrid functional.

3.2. TD-DFT absorption spectrum of $[Fe(phen)_3]^{2+}$

The lowest part of the absorption spectrum of the LS state contains basically three types of excitations: (i) ligand-field or metal centered (MC) transitions involving electron replacements within the Fe-3d orbitals; (ii) metal-to-ligand charge transfer transitions (MLCT) in which an electron is transferred from Fe to an antibonding orbital on the ligands and (iii) excitations entirely localized on the ligands, the ligand centered (LC) transitions involving the π and π^* orbitals of phenantroline. In addition to the relative energies and intensities of these transitions, we also establish to what extent the spectrum is affected by the inclusion of solvent effects.

First, we will make a complete analysis of the 40 lowest singlet excitations of the complex in vacuum and in solution (H_2O) using the TD-DFT method. Figure 3 summarizes in a graphical way the results by representing each transition with a gaussian-type function of full-width at half-maximum of 25 nm. The height of each peak is normalized to the peak with the largest oscillator strength. The top figure shows the results for **1** in vacuum, the colored thinner lines represent the individual transitions and the sum of these is represented with the thicker line. The calculated absorption spectrum shows three main absorption bands and also three less intense shoulders. The main

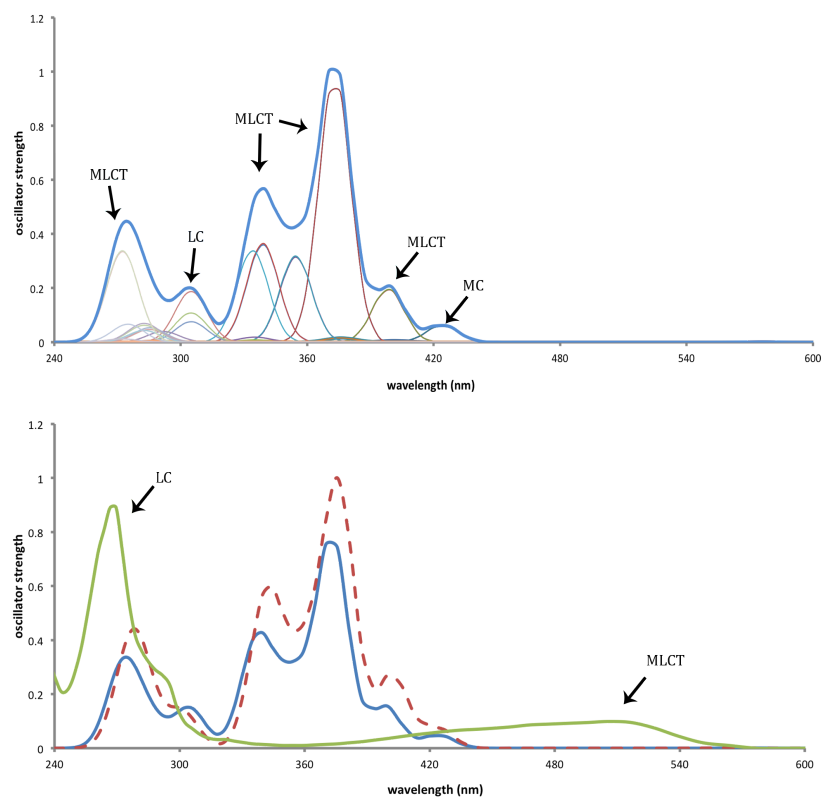


Figure 3: Top: TD-DFT PBE0/def2-TZVP absorption spectrum for $[\text{Fe}(\text{phen})_3]^{2+}$ in vacuum representing the transitions by a Gaussian function. Bottom: Comparison between vacuum (solid blue line), water (dashed line) and the experimental spectrum [16] (solid green line).

bands are localized around 270, 340 and 370 nm, and correspond to MLCT transitions that involve electron replacements in the Fe-3d orbitals and π^* ligand orbitals. The intensity of these bands is in concordance with their dipole allowed character. The band centered at 310 nm is formed by a collection of nearly degenerate ligand-centered transitions among the π and π^* orbitals of the ligand. These excitations are also optically allowed. PBE0/TD-DFT predicts a slightly less intense absorption with respect to the MLCT states, contrasting experimental data, which clearly point at more intense LC excitations [16]. Finally, the metal-centered Fe-3d transitions appear around 420 and 570 nm but they are very weak due to the nearly octahedral coordination sphere of the Fe^{2+} ion. Note that the absence of absorptions at shorter wave lengths ~ 260 nm is due to the limiting the calculation to the first 40 singlet states. Determining more roots would most probably lead to finite intensities at these shorter wave lengths.

The lower part of Figure 3 compares the vacuum calculation to the results obtained with solvent effects modelled with a COSMO representation of water. As can be seen, the effect of the environment on the excitation energies and intensities is rather small. The basic features of the spectrum are maintained and at this stage, we conclude that the solvent effects on the geometry, and the adiabatic and vertical excitation energies are small. However, there is an important issue that still needs to be resolved; the overall agreement between the TD-DFT and the experimental spectrum (green line in Figure 3, bottom) is not very satisfactory. Therefore, we checked the effect of the solvent on the excitation energies with CASPT2, which in principle should provide more accurate results.

3.3. CASPT2 absorption spectrum of $[\text{Fe}(\text{phen})_3]^{2+}$

From previous studies, it is well known that the optimal CASPT2 Fe–N distance does not necessarily coincide with the one of the optimized DFT geometry [18, 37, 50, 51]. Since the excitation energies are rather susceptible to this parameter (especially the MC excitations), we have manually determined the optimal CASPT2 distance in the field of DFT relaxed ligand geometries by generating a set of DFT optimized geometries with different Fe–N distances and calculated the CASPT2 energy of the LS state at all points with a CAS(10,12) reference wave function. Note that a full CASPT2 geometry optimization is computationally too expensive, and would probably not provide extra information. The multiconfigurational character of the wave function is basically related with the electronic configuration of Fe

and the Fe–N bond. The optimization of the ligand geometry with CASPT2 would not bring new information to that provided by DFT.

The scan of the Fe–N distance locates the optimal CASPT2 Fe–N distance at 1.92 Å, significantly shorter than obtained with DFT and determined from X-ray diffraction measurements. As can be seen in Table 1, the relative energies of the lowest d-d transitions strongly depend on the geometry. For shorter distances the ligand field is stronger and the MC excited states become higher in energy.

The full absorption spectrum was obtained in a two-step procedure. In the first place, we used the CAS(10,15) reference wave function to obtain simultaneously CASPT2 estimates of the MC and MLCT excitation energies and intensities. The LC excitations were subsequently added by performing CASPT2 calculations with the CAS(12,12) reference wave function and the results are summarized in Table 2. The lowest MLCT states appear around 2.60 eV, slightly higher than the spin allowed MC excitations. The oscillator strength of the latter is however two orders of magnitude smaller and is hardly detectable in the graphical representation of the CASPT2 absorption spectrum constructed in the same way as the PBE0/TD-DFT spectrum discussed above. MLCT states are found in a rather broad interval ranging from 475 nm to approximately 330 nm. At shorter wave length we find very intense LC excitations. Again, the results in vacuum (solid line) were compared to the results obtained after including solvent effects through a PCM treatment of water or acetonitrile (dashed curve, no difference between the two solvents). Whereas the relative energies of the transitions are hardly affected by the solvent, the oscillator strengths of some states is somewhat diminished, most specifically the states that contribute to the peak around 400 nm. Nevertheless, the overall shape of the absorption spectrum is maintained and the solvent effects are also small for the CASPT2 calculations

This brings us to the last point; the comparison of the CASPT2 results with the experimental spectrum, represented by the green thick line in Figure 4. The overall agreement is rather satisfactory and much better than the one obtained with TD-DFT/PBE0. The main features of the spectrum are correctly reproduced and the only obvious discrepancy lies in the on-set of the bands. Experimentally, the MLCT band starts around 550 nm (2.3 eV) and the LC band around 275 nm (4.5 eV), while CASPT2 places the on-set at 450 nm (2.6 eV) and 250 nm (4.96 eV), respectively. This behaviour is similar to the one observed in $[\text{Fe}(\text{bpy})_3]^{2+}$, where an almost identical difference in the lowest MLCT excitation energy was found [18, 52]. The error of 0.4 eV

Table 1: CASPT2 vertical transition energies (in eV) of the lowest electronic MC transitions of $[\text{Fe}(\text{phen})_3]^{2+}$ at the DFT optimized Fe-N distance (2.00 Å) and the CASPT2 optimal^(a) distance (1.92 Å). The reference wave function is obtained from a CAS(10,12) calculation. Results in parenthesis correspond to those obtained with the PCM solvent model for water.

State	DFT optimized	CASPT2 optimal ^(a)
	2.00 Å	1.92 Å
$^1\text{A}_{1g}$	0.00 (0.00)	0.00 (0.00)
$^5\text{T}_{2g}$	0.92 (0.92)	2.43 (2.43)
	0.93 (0.93)	2.43 (2.43)
	1.02 (1.02)	2.43 (2.43)
$^3\text{T}_{1g}$	0.99 (0.99)	1.71 (1.72)
	1.03 (1.03)	1.74 (1.74)
	1.03 (1.03)	1.80 (1.80)
$^3\text{T}_{2g}$	1.51 (1.51)	2.27 (2.27)
	1.53 (1.53)	2.30 (2.30)
	1.61 (1.61)	2.36 (2.36)
$^1\text{T}_{1g}$	1.91 (1.91)	2.62 (2.62)
	1.96 (1.96)	2.66 (2.66)
	1.97 (1.97)	2.69 (2.69)
^5E	3.44 (3.44)	5.65 (5.65)
	3.45 (3.45)	5.66 (5.66)

a: The optimal CASPT2 distance was obtained from a scan of the energy along a series of PBE0 optimized geometries restricting the Fe-N distance to a value in the range of 1.90-2.00 Å.

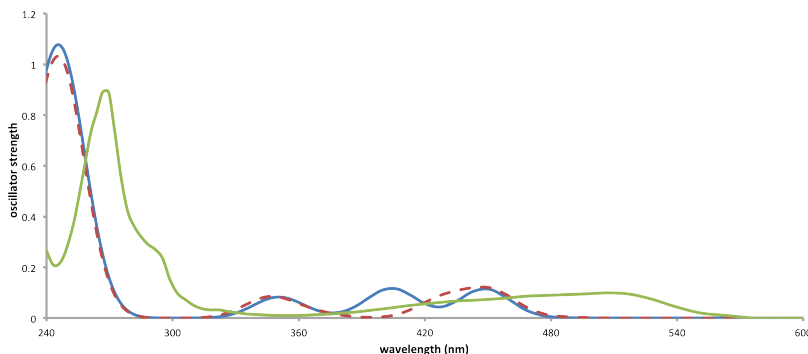


Figure 4: CASPT2 absorption spectrum of $[\text{Fe}(\text{phen})_3]^{2+}$ (**1**) representing the transitions by a Gaussian function (solid blue line) in vacuum and (dashed lines) in water. The solid green line represents the absorption spectrum obtained experimentally.

observed for the LC band may be reduced by considering a larger active space with more π orbitals. Eventually, one may have to perform restricted active space SCF (RASSCF) calculations [53] to treat the complete π system.

3.4. Solvent effects for $\text{trans}(\text{Cl})\text{-Fe}(\text{bpy})\text{Cl}_2(\text{CO})_2$ and $\text{trans}(\text{Cl})\text{-Ru}(\text{bpy})\text{Cl}_2(\text{CO})_2$

Although the results discussed so far indicate that the solvent effects on the absorption spectrum of $[\text{Fe}(\text{phen})_3]^{2+}$ are small, there are of course several cases where solvent effects play a very important role and cannot be omitted in the theoretical description of the electronic structure. A recent example is given by the calculations of Escudero and González on $\text{trans}(\text{Cl})\text{-Ru}(\text{bpy})\text{Cl}_2(\text{CO})_2$ [19]. The TD-DFT result with and without solvent effects show differences in the excitation energies as large as 1 eV. To double check the computational strategy applied here for $[\text{Fe}(\text{phen})_3]^{2+}$, we have applied it to the mentioned Ru complex (**3**) and to a variant of it, by changing Ru for Fe (**2**).

The geometry optimization of $\text{trans}(\text{Cl})\text{-Ru}(\text{bpy})\text{Cl}_2(\text{CO})_2$ with PBE0/TZVP gives accurate bond distances and angles (see supporting information). Hence, it is expected that the optimized geometry of the hypothetical complex $\text{trans}(\text{Cl})\text{-Fe}(\text{bpy})\text{Cl}_2(\text{CO})_2$ is also reasonable. Table 3 lists the TD-DFT results for **2** and **3** with and without solvent effects. The results for the Ru complex are in close agreement with those obtained by Escudero and González and important solvent effects are observed for some of the states. The largest changes in the excitation energies occur for the MLCT

Table 2: CASPT2 vertical excitation energies ΔE (in eV) of the lowest electronic transitions of $[\text{Fe}(\text{phen})_3]^{2+}$ (**1**). MC and MLCT are calculated with a CAS(10,15) reference wave function, and LLCT with a CAS(12,12) reference wave function.

State	ΔE (vacuum)	ΔE (water)
$^1\text{A}_{1g}$	0.00	0.00
1^1MC	2.59	2.59
1^1MLCT	2.60	2.58
2^1MLCT	2.77	2.74
3^1MLCT	3.06	2.89
4^1MLCT	3.08	3.35
5^1MLCT	3.29	3.24
2^1MC	3.54	3.58
1^1LLCT	5.20	5.26
2^1LLCT	5.21	5.30
3^1LLCT	5.32	5.43
3^1MC	5.53	5.53
4^1MC	5.60	5.60
5^1MC	5.67	5.66
6^1MC	5.81	5.82
4^1LLCT	6.26	6.27
5^1LLCT	6.33	6.30

states and less important effects are observed for the LC and MC excitations. The excitations in which an electron is transferred from Cl or CO to bipyridine (ligand-to-ligand charge transfer (LLCT)) are also affected, whereas the LLCT excitations among CO and Cl are not influenced by the solvent. A similar picture arises from the TD-DFT calculations on **2**: the relative energy for several MLCT states show large solvent effects, while this is less pronounced for the LC and MC states. As soon as the LLCT excitations involve bipyridine orbitals, the excitation energy is significantly blue-shifted. Note that in some cases the classification of the excitation as MLCT, LLCT, etc. is not straightforward, since the Kohn-Sham orbitals have a certain degree of delocalization and are not easily identified as Fe or ligand orbital. Moreover, many excitations show several contributions with similar weights.

Subsequently, we have applied the CASPT2 methodology to **2** and **3** and compared the vacuum results to those obtained with a PCM modelling of the solvent (water and acetonitrile). Table 4 summarizes the results obtained for both complexes. The MLCT states for **2** involve electron replacements from Fe to the antibonding orbitals of the CO ligands, while the excitations labeled as MLCT in **3** excite electrons from Ru to the π^* orbitals of pyridine. This is due to the impossibility to include empty orbitals of all the different ligands in the active space. The Ru-complex has low-lying pyridine orbitals, while for the Fe analogue the CO antibonding π^* orbitals enter the active space preferentially. In these complexes the LC and LLCT excitations have not been calculated. This would require a complete new CASSCF reference wave function as done for $[\text{Fe}(\text{phen})_3]^{2+}$, but not essential to illustrate the solvent effects in **2** and **3**.

The solvent effects calculated with CASPT2 are similar to those observed in the TD-DFT calculations, varying from approximately 0.1 eV for MC states to nearly 1 eV for the MLCT states of **3**, which involve the bipyridine ligand orbitals. The MLCT states in **2** are due to electron replacements from Fe to π^*_{CO} and their relative energy remain nearly constant when the solvent is added. Hence, the computational scheme is capable of accounting for solvent effects when they are present and the no appearance of these in **1** is not due to artefacts in the method.

An important parameter to explain the energy shifts is the dipole moment. In Table 5, we summarize the dipole moments calculated as the expectation value of the CASSCF wave function and the effect of the solvent on the relative energies for a collection of states in the three complexes considered. It is clear that changes in the excitation energy are closely related to the

difference of the dipole moment between ground and excited state. In the case of $[\text{Fe}(\text{phen})_3]^{2+}$, the ground state has an almost zero dipole moment and none of the excited states gains a large dipole moment. This is expected for the MC states, but less obvious for MLCT states. The antibonding π orbitals on the phenantroline ligands in the active space (those that become occupied in the MLCT states) are delocalized over one, two or three ligands. In all cases, the MLCT states are linear combinations of single electron replacements such that the overall transfer from the metal to the ligands is symmetric in all three directions, and hence, no dipole is induced by the excitation. This explains the minimal effect on the excitation energies when the solvent is included in the calculation. On the contrary, the less symmetric complexes **2** and **3** with three different ligands coordinating the metal have a large dipole moment in the ground state pointing from the metal to the bipyridine ligand. The dipole moment is largely canceled when an electron is transferred from the metal to the bipyridine ligand. This induces a large response of the solvent, and hence, shifts the excitation energy in comparison to the value calculated in vacuum. When the electron is excited to the antibonding orbitals of the CO ligands, the change in the dipole moment is smaller, which explains the weaker solvent effects for these MLCT states.

3.5. Orthogonal Valence Bond analysis of the wave function

Having confirmed that the solvent effects on the excitation energies are intimately related to changes in the dipole moment of the initial and final states involved in the transition, it is interesting to see whether the solvent has any effect on the electronic structure of the ground state. To this purpose, we analyze the wave function of the LS with and without solvent in the framework of orthogonal Valence Bond. Instead of the more common natural orbitals, the CASSCF wave function is expressed in localized orbitals obtained by a unitary transformation [47]. Using these localized orbitals (shown in the supporting information), it is possible to mark the configuration state functions of the CASSCF wave function by the number of electrons associated to the metal ion. This is not possible when the function is expressed in natural orbitals which are much more delocalized over metal and ligands.

Table 6 reports the decomposition of the LS wave function for all three compounds. It can be readily seen that there is practically no difference between the vacuum and solvent results. This indicates that the wave function of the fundamental state does not change when solvent effects are included in the electronic structure. More interesting is the comparison between the

Table 3: TD-DFT vertical excitation energies ΔE (in eV) of **2** and **3**. XLCT indicate charge transfer excitations involving the Cl ligand.

State	2		3	
	ΔE (vacuum)	ΔE (water)	ΔE (vacuum)	ΔE (water)
Ground state	0.00	0.00	0.00	0.00
1 ¹ XLCT/MLCT	2.66	3.71	2.36	3.33
$n_{\text{Cl}}/d_{\text{t}2\text{g}} \rightarrow \pi^*_{\text{bpy}}$				
2 ¹ XLCT/MLCT	2.74	4.19	2.49	3.47
$n_{\text{Cl}}/d_{\text{t}2\text{g}} \rightarrow \pi^*_{\text{bpy}}$				
1 ¹ XLCT/MC	2.95	3.17	3.95	4.28
$n_{\text{Cl}}/d_{\text{t}2\text{g}} \rightarrow \pi^*_{\text{CO}}/d_{\text{eg}}$				
2 ¹ XLCT/MC	3.11	3.31	4.10	4.44
$n_{\text{Cl}}/d_{\text{t}2\text{g}} \rightarrow \pi^*_{\text{CO}}/d_{\text{eg}}$				
1 ¹ LLCT	3.51	4.62		
$n_{\text{Cl}} \rightarrow \pi^*_{\text{bpy}}$				
1 ¹ MLCT	3.60	3.61		
$n_{\text{Cl}}/d_{\text{t}2\text{g}} \rightarrow \pi^*_{\text{CO}}$				
3 ¹ XLCT/MLCT	3.62	4.81	3.29	4.28
$n_{\text{Cl}}/d_{\text{t}2\text{g}} \rightarrow \pi^*_{\text{bpy}}$				
4 ¹ XLCT/MLCT	4.19	4.56	3.56	4.57
$n_{\text{Cl}}/d_{\text{t}2\text{g}} \rightarrow \pi^*_{\text{bpy}}$				
1 ¹ XLCT/LLCT	4.46	4.76	4.48	4.42
$n_{\text{Cl}}/d_{\text{t}2\text{g}} \rightarrow \pi^*_{\text{CO}}$				
$\pi_{\text{bpy}} \rightarrow \pi^*_{\text{bpy}}$				
2 ¹ XLCT/LLCT	4.58	5.04		
$n_{\text{Cl}}/d_{\text{t}2\text{g}} \rightarrow \pi^*_{\text{CO}}$				
$\pi_{\text{bpy}} \rightarrow \pi^*_{\text{bpy}}$				

Table 4: CASPT2 vertical transition energies ΔE (in eV) of **2** and **3**. The MLCT excitations in **2** correspond to excitations from Fe-3d(t_{2g}) to π_{CO}^* and in **3** to π_{bpy}^*

State	2		3	
	ΔE (vacuum)	ΔE (water)	ΔE (vacuum)	ΔE (water)
$^1A_{1g}$	0.00	0.00	0.00	0.00
1^1MC	2.34	2.30	4.15	4.24
2^1MC	3.76	3.85	4.01	4.24
3^1MC	3.38	3.53	4.51	5.19
4^1MC	4.15	3.99	5.14	5.51
1^1MLCT	4.38	4.50	3.87	4.84
2^1MLCT	4.61	4.60	3.90	4.64
3^1MLCT	5.29	5.30	4.59	5.39
4^1MLCT	5.92	5.92		

Table 5: Changes in the CASPT2 vertical transition energies $\Delta(\Delta E)$ (in eV) and the dipole moment $|\Delta\mu|$ (in Debye) of **1**, **2** and **3** between vacuum and solution.

State	1		2		3	
	$\Delta(\Delta E)$	$ \Delta\mu $	$\Delta(\Delta E)$	$ \Delta\mu $	$\Delta(\Delta E)$	$ \Delta\mu $
1^1MC	0.00	0.16	0.04	0.37	0.09	0.94
2^1MC	0.04	0.34	0.09	0.74	0.33	0.28
3^1MC	0.00	0.14	0.15	0.16	0.68	0.20
4^1MC	0.00	0.08	0.16	0.35	0.37	1.08
1^1MLCT	0.02	4.48	0.12	2.50	0.97	6.89
2^1MLCT	0.03	2.54	0.01	2.44	0.74	7.73
3^1MLCT	0.17	2.08	0.01	2.61	0.80	5.52
4^1MLCT	0.27	2.11	0.00	3.01		

Table 6: Orthogonal Valence Band decomposition of the CASSCF wave function of the LS state for **1**, **2** and **3** expressed in weights of different TM-dⁿ L^m electronic configurations (n+m equals the number of active electrons). Results in vacuum are compared with a PCM modelling of the solvent.

Complex		Electronic configuration				Total
		TM-d ⁶ L ⁴	TM-d ⁷ L ³	TM-d ⁸ L ²	TM-d ⁹ L ¹	
1	vacuum	55.0	33.9	8.3	2.1	99.3
	water	55.0	33.8	8.3	2.1	99.2
2	vacuum	18.7	44.7	26.0	8.0	97.4
	water	18.7	44.7	25.9	7.9	97.2
3	vacuum	9.7	39.9	38.3	11.2	99.1
	water	9.6	39.9	38.4	11.2	99.1

three different compounds. Assuming an ionic model with a formal TM(II) state, the TM-d⁶ state should be the leading electronic configuration. This is true to some extent for **1**, but cannot be maintained for the other two complexes. In these cases the CO ligand provides a much stronger σ donation than the phenantroline ligands, leading to very low weights of the ionic configuration. This effect is slightly stronger in the Ru complex due to the larger spatial extent of the TM-4d orbitals. The weight of the ionic determinant has been found to be an indication of the possibility for SCO [54]. Normally, SCO compounds have weights of roughly 55%. This is indeed compatible with the SCO character of **1**, while it excludes any kind of such phenomena for the other two complexes. The adiabatic energy difference between LS and HS is too large in these cases [54].

4. Conclusions

The purpose of this work was to investigate theoretically the solvent effects on the electronic states of [Fe(phen)₃]²⁺, trans(Cl)-Fe(bpy)Cl₂(CO)₂ and trans(Cl)-Ru(bpy)Cl₂(CO)₂, comparing (TD-)DFT to CASPT2 results. Because the results obtained with TD-DFT for all the transitions differ from the values obtained with CASPT2 and do not compare very favorably with the available experimental data, the hybrid TD-DFT/PBE0 cannot be recommended as an alternative for the study of the excited states in the present case. Note that a recent study on a related Fe(II) complex shows that the

pure density functional PBE performs much better than the hybrid variant used here [55]. More general conclusions about the suitability of TD-DFT to treat excited states in Fe(II)/Ru(II) (or other TM) complexes would require a more extensive study, which is beyond the scope of the present paper.

CASPT2 results of $[\text{Fe}(\text{phen})_3]^{2+}$ compare much better with experiment. The theoretical absorption spectrum places the MLCT and the LC bands slightly higher in energy than experimentally measured, which can be explained by the use of the ideal geometry in which the three phenantroline ligands are identical, leading to delocalized MLCT states with slightly higher energy than the ones that localize on one ligand.

The solvent effects were treated with the COSMO model for (TD-)DFT, and with PCM for the CASPT2 calculations. The results obtained show that solvent effects are only important when the dipole moment between initial and final state changes significantly. The transitions of $[\text{Fe}(\text{phen})_3]^{2+}$ are not affected by the introduction of solvent effects due to the high symmetry of the complex. On the other hand, the MLCT of the complex 2, that involve the bipyridine ligand, are affected due the asymmetric charge transfer involved in these transitions. The excitations that involve the carbonyl ligand, which do not show significant changes in dipole moment, are hardly affected by adding solvent effects. It should be kept in mind that thermal motion of the complexes and the solvent molecules around these will continuously break the highly symmetric average structure [56]. Hence, solvent effects are important, although one has to find a way to efficiently take into account the effect of the thermal motion in the calculation of the spectrum [57]. Furthermore, it should be kept in mind that the continuum models for the solvent used in the present study may not be the most accurate representation in case of protic solvents [58, 59]. It cannot be discarded that the explicit inclusion of the first solvation sphere of the complex in the calculation provides a better agreement with experiment.

Finally, an analysis of the wave function has been done using orthogonal Valence Bond theory. Two conclusions were obtained with this analysis: (i) the wave function of the ground state does not suffer changes when the solvent effects are included and (ii) the weight of the ligand-to-metal charge transfer (LMCT) determinants is an indication of a possible thermal SCO. When the LS wave function has a contribution of approximately 45% of the LMCT, the complex is susceptible to thermal SCO.

Acknowledgments: Financial support has been provided by the Spanish Administration (Project CTQ2011-23140), the Generalitat de Catalunya (Projects 2009SGR462 and Xarxa d'R+D+I en Química Teòrica i Computacional, XRQTC) and the European Union (COST Action CODECS CM1002).

- [1] J. J. McGarvey, I. Lawthers, *J. Chem. Soc., Chem. Commun.* (1982) 906–907.
- [2] S. Decurtins, P. Güttlich, C. P. Köhler, H. Spiering, A. Hauser, *Chem. Phys. Lett.* 105 (1) (1984) 4.
- [3] A. Hauser, *J. Chem. Phys.* 94 (1991) 2741–2748.
- [4] A. Hauser, C. Enachescu, L. M. Lawson Daku, A. Vargas, N. Amstutz, *Coord. Chem. Rev.* 250 (2006) 1642–1652.
- [5] J.-F. Létard, *J. Mater. Chem.* 16 (2006) 2550–2559.
- [6] M. A. Halcrow, *Chem. Soc. Rev.* 37 (2008) 278–289.
- [7] C. Boilleau, N. Suaud, N. Guihéry, *J. Chem. Phys.* 137 (2012) 224304.
- [8] H. Paulsen, L. Duelund, H. Winkler, H. Toftlund, A. Trautwein, *Inorg. Chem.* 40 (9) (2001) 2201–2203.
- [9] M. Reiher, O. Salomon, B. A. Hess, *Theor. Chem. Acc.* 107 (1) (2001) 48–55.
- [10] M. Swart, A. W. Ehlers, K. Lammertsma, *Mol. Phys.* 102 (23-24) (2004) 2467–2474.
- [11] M. Swart, A. R. Groenhof, A. W. Ehlers, K. Lammertsma, *J. Phys. Chem. A* 108 (25) (2004) 5479–5483.
- [12] B. O. Roos, P. R. Taylor, P. E. M. Siegbahn, *Chem. Phys.* 48 (2) (1980) 157–173.
- [13] K. Andersson, P.-A. Malmqvist, B. O. Roos, *J. Chem. Phys.* 96 (2) (1992) 1218–1226.

- [14] M. Kepenekian, B. Le Guennic, V. Robert, *J. Am. Chem. Soc.* 131 (2009) 11498–11502.
- [15] B. Le Guennic, S. A. Borshch, V. Robert, *Inorg. Chem.* 46 (2007) 11106–11111.
- [16] J. Tribollet, G. Galle, G. Jonusauskas, D. Deldicque, M. Tondusson, J.-F. Letard, E. Freysz, *Chem. Phys. Lett.* 513 (1-3) (2011) 42–47.
- [17] W. Gawelda, A. Cannizzo, V.-T. Pham, F. van Mourik, C. Bressler, M. Chergui, *J. Am. Chem. Soc.* 129 (26) (2007) 8199–8206.
- [18] C. de Graaf, C. Sousa, *Chem. Eur. J.* 16 (15) (2010) 4550–4556.
- [19] D. Escudero, L. González, *J. Chem. Theory Comput.* 8 (1) (2012) 203–213.
- [20] C. Adamo, V. Barone, *J. Chem. Phys.* 110 (13) (1999) 6158–6170.
- [21] M. Pápai, G. Vankó, C. de Graaf, T. Rozgonyi, *J. Chem. Theory Comput.* 9 (1) (2013) 509–519.
- [22] L. M. Lawson Daku, A. Vargas, A. Hauser, A. Fouqueau, M. E. Casida, *ChemPhysChem* 6 (2005) 1393–1410.
- [23] F. Weigend, R. Ahlrichs, *Phys. Chem. Chem. Phys.* 7 (2005) 3297.
- [24] C. Ochsenfeld, J. Gauss, R. Ahlrichs, *J. Chem. Phys.* 103 (17) (1995) 7401–7407.
- [25] A. Klamt, G. Schuurmann, *J. Chem. Soc., Perkin Trans. 2* 0 (1993) 799–805.
- [26] M. Von Arnim, R. Ahlrichs, *J. Comput. Chem.* 19 (15) (1998) 1746–1757.
- [27] R. Ahlrichs, M. Bär, M. Häser, H. Horn, C. Kölmel, *Chem. Phys. Lett.* 162 (3) (1989) 165–169.
- [28] G. Karlström, R. Lindh, P.-Å. Malmqvist, B. O. Roos, U. Ryde, V. Veryazov, P.-O. Widmark, M. Cossi, B. Schimmelpfennig, P. Neogady, L. Seijo, *Comput. Mater. Sci.* 28 (2003) 222–239.

- [29] F. Aquilante, L. De Vico, N. Ferré, G. Ghigo, P.-Å. Malmqvist, P. Neogady, T. B. Pedersen, M. Pitoňák, M. Reiher, B. O. Roos, L. Serrano-Andrés, M. Urban, V. Veryazov, R. Lindh, *J. Comput. Chem.* 31 (2010) 224–247.
- [30] B. O. Roos, R. Lindh, P.-Å. Malmqvist, V. Veryazov, P.-O. Widmark, *J. Phys. Chem. A* 108 (2004) 2851–2858.
- [31] B. O. Roos, R. Lindh, P.-Å. Malmqvist, V. Veryazov, P.-O. Widmark, *J. Phys. Chem. A* 109 (2005) 6575–6579.
- [32] F. Aquilante, T. B. Pedersen, R. Lindh, *J. Chem. Phys.* 126 (2007) 194106.
- [33] F. Aquilante, P.-Å. Malmqvist, T. B. Pedersen, A. Ghosh, B. O. Roos, *J. Chem. Theory Comput.* 4 (2008) 694–702.
- [34] B. A. Hess, *Phys. Rev. A* 33 (1986) 3742–3748.
- [35] P.-Å. Malmqvist, B. O. Roos, B. Schimmelpfennig, *Chem. Phys. Lett.* 357 (2002) 230–240.
- [36] B. O. Roos, P.-Å. Malmqvist, *Phys. Chem. Chem. Phys.* 6 (2004) 2919–2927.
- [37] K. Pierloot, S. Vancoillie, *J. Chem. Phys.* 125 (2006) 124303.
- [38] N. Forsberg, P.-Å. Malmqvist, *Chem. Phys. Lett.* 274 (1997) 196–204.
- [39] G. Ghigo, B. O. Roos, P.-Å. Malmqvist, *Chem. Phys. Lett.* 396 (2004) 142–149.
- [40] M. Kepenekian, V. Robert, B. Le Guennic, *J. Chem. Phys.* 131 (2009) 114702.
- [41] L. M. Lawson Daku, F. Aquilante, T. W. Robinson, A. Hauser, *J. Chem. Theory Comput.* 8 (2012) 4216–4231.
- [42] M. Cossi, G. Scalmani, N. Rega, V. Barone, *J. Chem. Phys.* 117 (1) (2002) 43–54.
- [43] S. Miertuš, E. Scrocco, J. Tomasi, *Chem. Phys.* 55 (1) (1981) 117 – 129.

- [44] R. Cammi, J. Tomasi, *J. Comput. Chem.* 16 (12) (1995) 1449–1458.
- [45] C. Angeli, R. Cimiraglia, J.-P. Malrieu, *J. Chem. Educ.* 85 (2008) 150–158.
- [46] C. Angeli, C. J. Calzado, C. de Graaf, R. Caballol, *Phys. Chem. Chem. Phys.* 13 (2011) 14617–14628.
- [47] A. Sadoc, R. Broer, C. de Graaf, *J. Chem. Phys.* 126 (13) (2007) 134709.
- [48] S. Nozawa, T. Sato, M. Chollet, K. Ichiyana, A. Tomita, H. Fujii, S. Adachi, S. Koshihara, *J. Am. Chem. Soc.* 132 (1) (2010) 61–63.
- [49] M. Swart, *J. Chem. Theory Comput.* 4 (12) (2008) 2057–2066.
- [50] B. Ordejón, C. de Graaf, C. Sousa, *J. Am. Chem. Soc.* 130 (2008) 13961–13968.
- [51] N. Suaud, M.-L. Bonnet, C. Boilleau, P. Labèguerie, N. Guihéry, *J. Am. Chem. Soc.* 131 (2009) 715–722.
- [52] C. Sousa, C. de Graaf, A. Rudavskiy, R. Broer, J. Tatchen, M. Etinski, C. M. Marian, *Chem. Eur. J.* (2013) in press (DOI: 10.1002/chem.201302992).
- [53] M. Merchán, E. Ortí, B. O. Roos, *Chem. Phys. Lett.* 226 (1994) 27–36.
- [54] A. Domingo, M. A. Carvajal, C. de Graaf, *Int. J. Quantum Chem.* 110 (2010) 331–337.
- [55] I. Georgieva, A. J. A. Aquino, N. Trendafilova, P. S. Santos, H. Lischka, *Inorg. Chem.* 49 (2010) 1634–1646.
- [56] M.-E. Moret, I. Tavernelli, M. Chergui, U. Rothlisberger, *Chem. Eur. J.* 16 (2010) 5889–5894.
- [57] A. Domingo, A. Rodríguez-Fortea, C. de Graaf, *J. Chem. Theory Comput.* 8 (2012) 235–244.
- [58] A. H. de Vries, P. T. van Duijnen, A. H. Juffer, *Int. J. Quantum Chem.: Quantum Chem. Symp.* 27 (1993) 451–466.
- [59] A. L. Barboza Formiga, S. Vancoillie, K. Pierloot, *Inorg. Chem.* 52 (2013) 10653–10663.